Epitaxial growth of tin oxide on Pt(111): Structure and properties of wetting layers and SnO_2 crystallites

Matthias Batzill,[1] Jooho Kim,[2] David E. Beck,[2] and Bruce E. Koel[2,*]
[1]*Department of Physics, Tulane University, New Orleans, Louisiana 70118, USA*
[2]*Department of Chemistry, University of Southern California, Los Angeles, California 90089-0482, USA*
(Received 20 November 2003; published 2 April 2004)

Tin-oxide films were grown on Pt(111) substrates by oxidation of Sn/Pt surface alloys using NO_2 exposures or by deposition of Sn in an NO_2 ambient gas. Structural aspects of monolayer tin-oxide films were reported previously [Phys. Rev. B **64**, 245402/1 (2001)]. At elevated substrate temperatures, growth of tin-oxide multilayers proceeds in a Stranski-Krastanov mode, i.e., the Pt substrate is covered with a monolayer thick tin-oxide wetting-layer before Sn-oxide crystallites form. The crystallites were tens to hundreds of nanometers in lateral size and were identified by scanning tunneling microscopy to be rutile SnO_2. These had a height of a few monolayers exposing the (011) crystal plane parallel to the Pt substrate. The low misfit of this crystal face with respect to the Pt(111) lattice apparently stabilizes this plane which is otherwise relatively energetically unfavorable. These studies demonstrate the importance of metal substrates in imposing structure and crystallographic orientation on oxide films. X-ray photoelectron spectroscopy studies of the tin-oxide films confirmed the existence of three Sn states that have been labeled previously as metallic, ''quasimetallic,'' and oxidic Sn. We conclude that the ''quasimetallic'' state results from oxidized Sn that is still alloyed within the Pt surface layer. Ultraviolet photoelectron spectroscopy of the valance band and electron energy loss spectroscopy confirmed a SnO_2 stoichiometry for multilayer tin-oxide films. High-resolution electron energy loss spectroscopy was used to identify characteristic vibrational modes for the different monolayer films. The SnO_2 crystallites, although only a few monolayers high and tens of nanometers in width, exhibit bulklike vibrational and electronic properties.

DOI: 10.1103/PhysRevB.69.165403 PACS number(s): 68.55.Jk, 68.35.−p, 73.22.−f

I. INTRODUCTION

Interfaces, regions of transition from one material to another, often exhibit structures and properties that are different from the bulk planes of materials. This is a result of adjustments of the atoms at the interface to minimize new free energy boundary conditions and smoothen alterations in electronic structure, e.g., ionic character, of materials across the interface. This may result in distinct structure and properties of the interface region. Similar to that at surfaces, i.e., the interface between a condensed phase and gas or vacuum, broken bonds may result in reordering at the interface compared to bulk planes. In contrast to surfaces, however, interfaces allow for new bonds to be formed between atoms in the two adjacent materials. This may result for epitaxial systems in interface structures that are different from any bulk planes of either material. Such interface structures may extend over several atomic layers and impose a different structure and/or crystallographic orientation of multilayer films from that of bulk structures or films that are not in contact with a dissimilar material. Monolayer films are a special class of interfaces that may differ yet from interfaces between two bulk materials. This is because monolayers have altered bonding environments on both sides of the layer, i.e., towards the substrate and the gas/vacuum for a monolayer surface.

Monolayers are an interesting subset of interfaces for several reasons. Notably, they provide the only interface that is directly accessible by a variety of surface science techniques that can be used to obtain information about these interfaces. Also, monolayers constitute an important class of surfaces that are different from bulk surfaces. Since most interactions of materials with the environment take place at surfaces, these unique surfaces are relevant to important materials problems related to coatings, sensors, and catalysts.

Here we report on studies of a metal/metal-oxide interface. Such investigations of metal oxide interfaces are complicated by the fact that oxides can exist with numerous stoichiometries and structures in their bulk form already. At interfaces between a metal-oxide and a dissimilar metal substrate, it is impossible to predict what stable interface structure will be formed. Frequently, more than one stable and/or metastable structure is observed, depending only on subtle differences in the preparation of the sample. The variety of these different structures however may not just be a nuisance, but enriches the number of materials with special properties that can be fabricated and exploited for devices. In fact some of these metal/oxide interfaces may already unknowingly play an important role in sensors and catalysts, e.g., due to the so-called strong metal support interaction (SMSI). This phenomenon has been known for a long time and plays an important role in the chemistry of dispersed metal nanoclusters on certain oxide supports common for commercial catalysts. Due to this interaction these metal clusters may be encapsulated in an oxide layer that profoundly changes the catalyst activity and selectivity. Recently the TiO_x film that formed on top of Pt metal clusters was imaged and characterized in an scanning tuneling microscopy (STM) study of platinum clusters supported on titania.[1,2]

We have described the structure of monolayer tin-oxide films formed on Pt(111) surfaces in a recent article.[3] These films were formed by oxidizing a Sn/Pt(111) surface alloy or a submonolayer Sn film with NO_2. NO_2 is a far more efficient oxidant than O_2 and no contamination of the surface with nitrogen was observed. STM, low-energy electron diffraction (LEED), and Auger electron spectroscopy (AES) were employed to characterize various metastable and stable oxide films. Three particular films were distinguished and structural models were proposed. In this article some of these structures are revisited and further characterized by vibrational and electronic spectroscopy. Furthermore, we extend these studies from monolayer tin-oxide films to multilayer films. We show that Sn-oxide films grow in a Stranski-Krastanov growth mode, i.e., Sn-oxide crystallites form after completion of a wetting layer. In particular, we attempt to elucidate the structure adopted by the multilayer film and how strong is the influence of the substrate on the structure and orientation of the oxide crystallites. These multilayer oxide films were characterized by STM, high-resolution electron energy loss spectroscopy (HREELS), UV photoelectron spectroscopy (UPS), and x-ray photoelectron spectroscopy (XPS).

In this context, multilayer growth of oxide films on metal substrates has been studied previously. Growth of iron oxide on Pt(111) was found to proceed in a Stranski-Krastanov growth mode.[4,5] Also, the growth of tin oxide on Au(111) substrates has been studied.[6] An ordered $c(2\times4)$ pattern with respect to the Au(111) surface was observed in LEED if Sn was oxidized at elevated temperatures. It was concluded that such films had a SnO_2 stoichiometry by using EELS. Studies on monolayer oxide films on metal substrates are much more numerous. A comprehensive list of references on such films has been given in our previous article.[3] For completeness, we add here that there also have been studies recently on the growth of vanadium oxide on Pd(111) (Refs. 7, 8) and of iron oxide,[9] titanium oxide,[10] and tin oxide[11] on Pt(100). Also, recent studies on the oxidation of bulk $Pt_3Sn(111)$ alloys were performed.[12,13] Oxidation of the bulk-alloy gave rise to very similar structures as those reported in Ref. 3 for SnO_x overlayers on Pt(111) surfaces.

II. EXPERIMENTAL METHODS

The experiments described in this article were performed in two UHV chambers, which are briefly described below. The tin-oxide monolayer films described previously[3] were characterized in the STM chamber and are not discussed in this article in any further detail. Here, results on tin-oxide multilayer film growth and structural characterization were obtained in the same STM apparatus as for the monolayer film studies. AES and LEED were the common techniques used in both UHV chambers to ensure that the same tin-oxide structures were being investigated. As described in detail in Ref. 3, different tin-oxide monolayers exhibit distinct LEED patterns that make it possible to identify the different structures. However, the complexity of the surface structures and preparation conditions causes some ambiguities in the comparison of the surfaces prepared in each chamber.

Two Pt(111) single crystals were used, one in each of the two chambers. The Pt(111) single crystals were prepared by using similar procedures and cleaned by a standard procedure consisting of cycles of 500-eV Ar^+-ion sputtering, annealing at 1000 K in 2×10^{-7} Torr O_2, and finally annealing at 1200 K in UHV. The cleanliness of the sample surface was monitored by AES. The sample temperature was monitored by a chromel/alumel thermocouple spotwelded directly to the side of the Pt(111) crystal. The same procedures described in Ref. 3 were used to form monolayer oxide films. Briefly, a $(\sqrt{3}\times\sqrt{3})R30°$ Sn/Pt(111) surface alloy was created by depositing ~1-ML Sn on the Pt(111) crystal at 300 K and subsequently annealing to 1000 K for 10 s.[14] This surface was then oxidized by exposure to 4×10^{-8} Torr NO_2 for 40 s at a sample temperature of 400 K. This temperature was chosen to avoid NO adsorption on the surface. No nitrogen contamination of the surface was subsequently detected in AES. In reporting the NO_2 exposures, no account was taken either for the ion gauge sensitivity or enhancement factor for the directed gas dosers. Tin-oxide multilayer films were grown at a sample temperature of 600 K by depositing Sn in a background pressure of 1×10^{-7} Torr NO_2.

A. STM chamber

The STM chamber is described in detail in Ref. 15. It is equipped with a double-pass cylindrical mirror analyzer (CMA) for AES, rear-view LEED optics, quadrupole mass spectrometer (QMS) for residual gas analysis and temperature programmed desorption (TPD), home-built single-piezo-tube STM, ion-gun for sample cleaning, resistively heated, Sn-evaporation source, and precision leak valves for gas dosing, including one directed-beam gas-doser for NO_2 exposures. The sample was heated by electron-beam heating from the backside of the Pt(111) crystal.

B. HREELS chamber

Experiments using EELS, HREELS, XPS, and UPS were conducted in a three-level UHV chamber, which has been described previously in Ref. 16. The top level was equipped with a double-pass CMA that was used for AES, XPS, and UPS. The x-ray and UV sources were mounted at 90° and 71.5° angles with respect to the CMA axis, respectively. The middle level was equipped with a front-view LEED optics and a QMS for TPD and residual gas analysis. The bottom level contained a LK2000 spectrometer for HREELS and EELS studies. A resistively heated, Ta boat for Sn dosing and a stainless steel gas dosing line connected to a precision leak valve for NO_2 dosing were situated in between the first and the second level. The Pt(111) crystal was mounted on two Ta rods that allowed for LN_2 cooling and resistive heating of the crystal. The sample could be transferred to different levels by a differentially pumped XYZ manipulator that also allowed polar rotation of the sample.

XPS data were obtained using Mg K_α x rays (1253.6 eV) with the CMA set to 25-eV pass energy for an analyzer resolution of 0.1 eV. Data were collected at two sample-analyzer geometries. One, the ''normal'' angle geometry, with the sample normal at 35° to the CMA axis, was chosen to maxi-

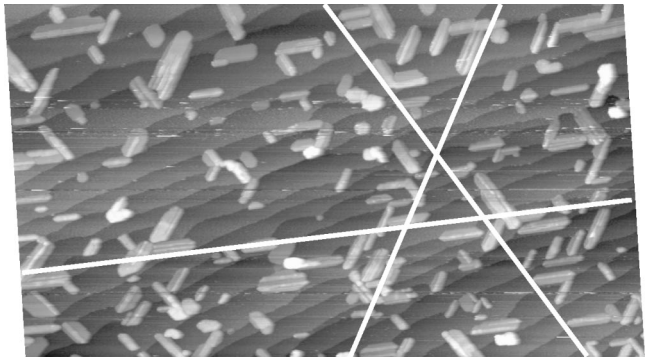

FIG. 1. Drift-compensated, large-scale STM image of a multilayer tin-oxide film on Pt(111) after annealing to 900 K. The image size is (470×280) nm^2. White lines are superimposed on the image to indicate the low index $\langle 110\rangle$ directions on the Pt(111) substrate. The tin-oxide crystallites are also aligned along these directions ($V_{\text{bias}}=-0.8$ V, $I=0.5$ nA).

mize the collected photoelectrons. Another geometry, at a ''glancing'' angle, was adopted to increase the surface sensitivity at the expense of total intensity with the sample surface normal at 80° to the CMA axis.

He(I) and He(II) UV photoelectron spectra were obtained using a high-pressure discharge lamp. The spectra were acquired at an analyzer pass energy of 25 eV for a resolution of 0.5 eV.

High-resolution electron energy loss spectra were recorded in the specular direction at an angle of 60° from the surface normal and incident beam energy of $E_p=4.53$ eV. Electron energy loss spectra were also recorded with the same geometry but at higher electron incident energies of $E_p=30$ eV and $E_p=100$ eV.

III. RESULTS AND DISCUSSION

Sn-oxide layers on Pt(111) were characterized by several different techniques, and the data obtained by each technique are presented and discussed separately below.

A. Scanning tunneling microscopy (STM)

Tin-oxide multilayer films were grown by Sn deposition on Pt(111) surfaces at 600 K in the presence of a NO_2 background pressure and subsequently annealed in vacuum to 900 K. After annealing a (4×4) LEED pattern was observed. STM shows that the surface consists of two structures: (i) a monolayer ''wetting'' layer of tin oxide that covers the whole surface and (ii) 3D crystallites of tin oxide. These two distinct structures are dealt with in the next two subsections.

1. SnO_2 *crystallites*

A large-scale STM image of this surface is shown in Fig. 1. The surface is covered with tin-oxide islands. These islands have an elongated shape, tens of nanometers wide and hundreds of nanometers long. The long axes of the islands are orientated along three symmetry directions of the Pt(111) substrate.

The atomic height steps that run across the substrate surface as imaged in Fig. 1 are similar to those observed for the clean Pt(111) surface. However, the tin-oxide islands sometimes appear to pin step edges, causing larger step edge curvature close to these pinning points. There is no evidence that the Pt-step edges act as preferred nucleation centers for tin-oxide islands.

Higher magnification of the tin-oxide islands is shown in Fig. 2(a). These islands exhibit a crystalline structure with defined angles between facets. The top facet of the crystal-

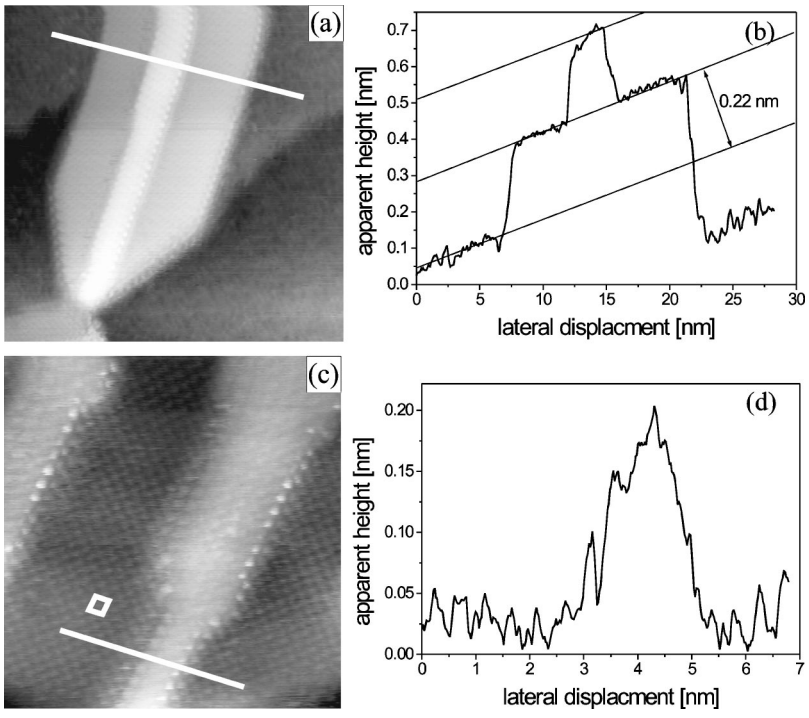

FIG. 2. STM images of SnO_2 crystallites. (a) ''Close-up'' view of a single tin-oxide crystallite. Imaged area is $(32\text{ nm})^2$, $V_{\text{bias}}=-0.75$ V, $I=0.55$ nA. (b) Cross section along the line indicated in (a). (c) STM image of the top face of a single crystallite. The unit cell of the atomic corrugation is indicated by the white rectangle. Imaged area is $(11\text{ nm})^2$, $V_{\text{bias}}=-0.2$ V, $I=0.1$ nA. (d) Cross section along the line in (c). This line scan shows an atomic corrugation of ~0.3 Å.

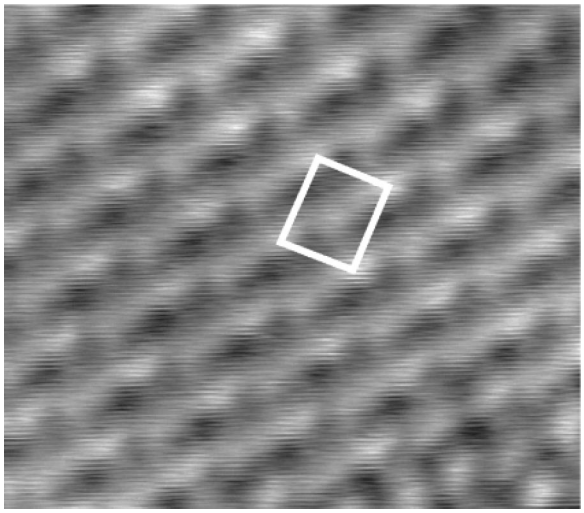

FIG. 3. High-resolution STM image of the surface of a crystallite. Two apparent heights in the atomic corrugation can be observed. This results in a unit cell indicated by the white rectangle. This unit cell is 0.48 ± 0.04 nm$\times0.56\pm0.05$ nm in size. Imaged area: (3.5×3.1) nm^2, $V_{bias}=-26$ mV, $I=0.65$ nA.

lites is parallel to the Pt substrate. The inclination of the side facets towards the substrate cannot be judged from the STM images due to the small height of the crystallites and because of tip-sample convolution effects. The apparent height of the crystallites as measured in the cross section in Fig. 2(b) indicates that the crystallites consist of 2–3 atomic layers. Terraces with step heights of 0.22 nm on top of the crystallites are observed often in agreement with step heights expected for monomolecular height steps. These terraces are narrow and run along the long axis of the crystallites with their step edges parallel to long edges of the crystallites. Brighter protrusions along the step edges are imaged by STM. We propose that these features are Sn atoms with reduced coordination to oxygen atoms. This makes them more metallic in character and increases their apparent height in STM images.

Atomic resolution images on top of the crystallites show that the edges of the crystallites are parallel to atomic rows, as is apparent in Fig. 2(a). This implies that the facets of the crystallites are low index faces of the crystalline structure. Figure 2(c) shows a STM image taken on top of a crystallite that exposes two terraces. Atomic corrugation can be observed on these terraces and these protrusions form a rectangular structure. The corrugation of these protrusions is about 0.3 Å as can be judged from the cross section displayed in Fig. 2(d).

Figure 3 shows an atomic resolution STM image taken at a low bias voltage on top of a crystallite. Two kinds of atomic protrusions are discriminated at these tunneling conditions. This allows one to draw a unit cell with bright protrusions in the corner and a darker one in the center as is indicated in the STM image. The sides of this rectangular unit cell is 0.48 ± 0.04 nm$\times0.56\pm0.05$ nm. This matches very well the unit cell for the rutile $SnO_2(011)$ surface. Furthermore, the observed atomic contrast in the STM images is also in good agreement with STM studies of bulk $SnO_2(011)$ surfaces.[17] The rutile SnO_2 structure and the (011) plane are

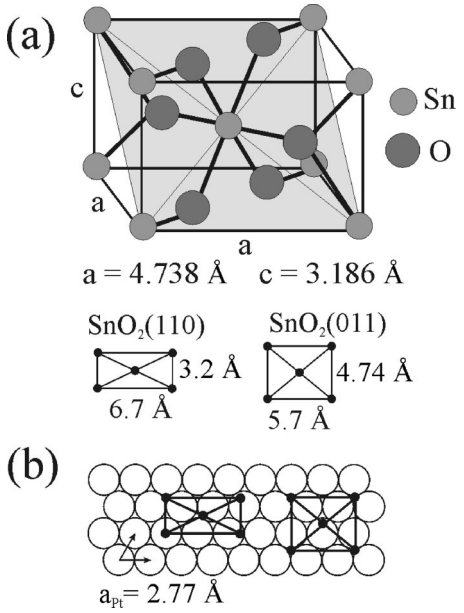

FIG. 4. (a) Crystal structure of rutile SnO_2. The (011) face is indicated by the gray plane. Unit cells for the (110) and the (011) surfaces are also shown. (b) Unit cells of the (110) and (011) SnO_2 surfaces are shown superimposed on a Pt(111) surface.

shown in Fig. 4. The (011) face has a rectangular unit cell with a size of 0.474 nm$\times$0.57 nm. Previously we reported that a tin-oxide monolayer structure existed on Pt(111) that could be constructed out of rectangular ''building'' blocks of $SnO_2(011)$ unit cells.[3] The $SnO_2(011)$ face fits the Pt(111) lattice very well, as demonstrated in Fig. 4(b). Placing the corners of the rectangular unit cell, i.e., Sn atoms, in threefold hollow sites of the Pt(111) substrate results in a rectangle that is 0.481 nm$\times$0.556 nm. This unit cell requires only a small expansion of 1.6% along the short side and a compression of 2.5% along the long side of the $SnO_2(011)$ unit cell. Thus, the Pt(111) substrate is lattice-matched quite well with the rutile $SnO_2(011)$ face. Good lattice matching reduces the interface energy between the tin-oxide crystallite and the Pt(111) substrate and thus stabilizes the crystallite face that matches the substrate surface lattice most closely. Therefore, the rutile $SnO_2(011)$ surface is exposed, although this is not the oxide surface with the lowest free energy. The (110) surface is the lowest energy, and most frequently studied, SnO_2 surface. First principle calculations for the surface energies of the low index surfaces of rutile SnO_2 indicate the (110) face as the most, the (100) the second, the (011) the third, and the (001) as the least stable surface.[18] The energy difference between the (110) and (011) surface is 28%, clearly favoring the (110) face. However, both the (110) and the (100) surfaces, which have lower surface energies than the (011) surface, do not fit well with the Pt(111) surface lattice. This is also indicated in Fig. 4(b). The dominant role of the Pt(111) substrate in controlling the orientation of the tin-oxide crystallites is seen not only from their surface termination but also from the strict alignment of the crystallites along the three symmetry directions of the Pt(111) substrate.

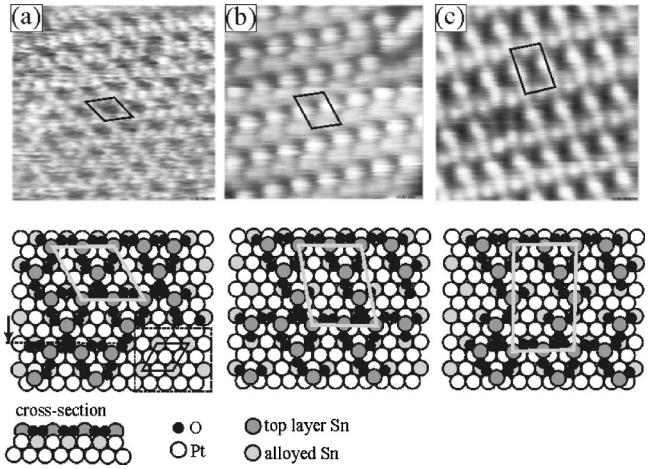

FIG. 5. STM images and schematic models for the wetting layer. All STM images are the same size $(8\,\mathrm{nm})^2$. (a) The surface exhibits a sixfold symmetric (4×4) structure. (b) and (c) show surfaces with 6 and 8 times the substrate lattice separation between ''beaded'' rows (see text for explanation). Unit cells are indicated for all three structures. The models discriminate between two Sn species: Sn present in the alloy surface and in the adlayer. Oxygen is bound to both Sn species. The alloy forms a (2×2) structure on the Pt(111) substrate.

2. Tin-oxide monolayer or "wetting" layer structure

Although the large scale STM image in Fig. 1 showed atomic steplike features on the Pt(111) substrate, closer investigations of the terraces in between the tin-oxide crystallites revealed that the surface was covered with a periodic structure larger than the Pt lattice. This structure exhibited many defects, but often could be identified as one of the structures that was previously observed following oxidation of Sn/Pt(111) surface alloys. This is also the structure that gives rise to the (4×4) LEED pattern observed for this surface. This (4×4) tin-oxide monolayer structure was described in detail in Ref. 3. A (4×4) superstructure was also reported for the oxidation of a bulk-$Sn_3Pt(111)$ alloy.[12,13] It is evident that this structure acts as a wetting layer for the multilayer film growth described here. This implies that the growth of thick Sn-oxide films proceeds first by covering the Pt(111) surface with a (4×4) or (4×4)-like structure, lowering the surface free energy of the system, and then forming 3D Sn-oxide crystallites. Thus, tin-oxide films grow on Pt(111) in a Stranski-Krastanov growth mode.

In addition to the (4×4) structure discussed above, two other ordered structures that are closely related to the (4×4) structure were found at this surface by using STM. STM images of all of these structures are shown in Fig. 5. All three structures exhibit rows with protrusions (beads) that exhibit a $2\times a_{\mathrm{Pt}}$ periodicity in the $\langle011\rangle$ direction on the Pt(111) surface. We call these ''beaded rows'' in the following discussion. However, the separation between these beaded rows in the $\langle101\rangle$ or $\langle-110\rangle$ directions are different for the three structures. This separation is $4\times a_{\mathrm{Pt}}$ for the (4×4) structure and 6 and $8\times a_{\mathrm{Pt}}$ for the other two structures, respectively. All three structures have features between these rows with a periodicity of $4\times a_{\mathrm{Pt}}$ in the same $\langle011\rangle$ direction as the orientation of the beaded rows. For the (4×4) structure, these features are identical to those observed within the beaded rows and this results in a threefold symmetric structure with the $\langle011\rangle$ direction indistinguishable from the $\langle101\rangle$ or $\langle-110\rangle$ directions. Therefore, this structure can be described as beaded rows in all three directions. This symmetry is broken for the other two structures, and the features between the rows appear more dominant in STM images although they have the same periodicity. It was speculated previously that the protrusions in the (4×4) structure were due to Sn—O ''pseudomolecules'' and ordering was a consequence of a closely packed structure of these pseudomolecules on specific adsorption sites on the Pt(111) surface. Observation of these two new, more open structures suggests a different interpretation as a structure that has some interlinking between the protrusions observed in STM.

Strings of alternating metal (M) and oxygen (O) atoms were observed previously after oxidation of single-component metal surfaces such as Cu(110),[19] Ag(110),[20] and Ni(110).[21] Also, —Cu—O— strings could be formed on Ag(110).[22] Thus, we speculate that the beaded rows are —Sn—O— strings. For Cu, Ag, and Ni (110) surfaces, these strings run along [100] directions and the metal atoms are separated by one lattice constant. The (110) surfaces also expose the separation by a factor of $1/\sqrt{2}$ closer packed [110] crystallographic direction such as on the (111) faces. No —M—O— strings were observed along these directions, indicating that the separation between the atoms along [110] directions is too short for forming a coincidence —M—O— string on the surface. On the (111) surface, however, only [110] low symmetry rows of atoms are accessible. Similar to the (110) faces it appears that the separation between two substrate atoms along these directions is too short for forming a —Sn—O— string with a separation between these Sn atoms of a single substrate atom. Thus, it is not surprising that the beads in our observations exhibit a separation of twice the substrate lattice. This is a long separation of $2\times a_{\mathrm{Pt}}=0.554\,\mathrm{nm}$ for Sn atoms in a —Sn—O— string though. Therefore, we speculate that Sn alloyed in the Pt substrate may be important to bridge this large separation. The possibility of forming an ordered (2×2) Sn/Pt interface alloy under these conditions was discussed previously.[3] The Sn necessary to form such a structure can be provided by Sn segregation from the bulk. This is consistent with the XPS data discussed below that indicate segregation of metallic Sn from the bulk to the surface region. Such an ordered alloy would also be a coincidence structure with the (4×4) oxide overlayer. Furthermore, formation of the (2×2) alloy may explain the apparently fundamental distance of two times the lattice constant for formation of the three different structures we have observed. Models are proposed for these three structures in Fig. 5. For the (4×4) structure, the model predicts a stoichiometry of Sn_7O_9 counting both Sn species in the overlayer as well as in the (2×2) alloy. Further support for the direct involvement of alloyed Sn comes from XPS studies that are described below that indicate a different chemical shift for alloyed Sn bonded to oxygen than the oxidized Sn present on top of the Pt substrate.

B. X-ray photoelectron spectroscopy (XPS)

XPS spectra were taken after various annealing temperatures for the oxidized surface alloy and after repeated oxidation and annealing of these surfaces. In addition, XPS data were collected for multilayer tin-oxide films obtained by Sn deposition in a background of NO_2 gas. All binding energies (BE's) are referenced to the Pt $4f_{7/2}$ peak set to 71.4 eV for clean Pt(111). Alloying Sn to form the (2×2) and $(\sqrt{3}\times\sqrt{3})R30°$ Sn/Pt(111) surface alloys caused no measurable shift in the Pt $4f_{7/2}$ peak and the Sn $3d_{5/2}$ peak appears at 484.6 eV BE.[23,24] No shift in the Pt $4f_{5/2}$ and $4f_{7/2}$ peaks after oxidation of the alloy surfaces or Sn oxide film growth was observed in this work. In the previous work using ozone for oxidation a shift of the Pt peaks was observed.[25] Ozone is a more efficient oxidant than NO_2, and thus it is quite possible that Pt was oxidized to a larger extent in those studies than in the experiments reported here.

Discrimination between SnO and SnO_2 is a difficult task by XPS. This is because only a small, and often disputed, shift of 0.7 eV occurs in the Sn $3d$ photoelectron peak between Sn^{2+} and Sn^{4+}.[26–29] Thin oxide-films can show additional shifts due to the interaction of the oxide layer with the substrate. For example, the influence of SiO_2 and MgO substrates on SnO and SnO_2 films was studied.[30–32] It was found that the Sn peak shifts to lower binding energies for increasing film thickness, i.e., Sn peaks for SnO and SnO_2 appear at higher binding energies in ultrathin films on these substrates. A Sn-$3d_{5/2}$ peak at 486.3 eV BE has been reported for bulk SnO_2.[26]

Sn XPS spectra for normal and glancing exit angles for monolayer and multilayer tin-oxide films on Pt(111) are displayed in Fig. 6. The Sn peaks were deconvoluted into three peaks. In order to determine the peak position for metallic Sn we deposited ~1.5 ML Sn on the Pt substrate at 300 K. This resulted in a Sn adlayer. The XPS spectrum of this sample has a Sn-$3d_{5/2}$ peak at 484.4 eV. If this Sn film is annealed and a Sn/Pt surface alloy is formed, then this peak shifts by 0.2 to 484.6 eV. The latter is the Sn peak we call the metallic Sn peak in the following. This is justified by the assumption that metallic Sn only exists as an alloy with Pt and not in an overlayer after oxidizing and annealing of the samples. The position for the most oxidic Sn $3d_{5/2}$ peak was determined from the multilayer Sn-oxide films prepared by Sn deposition in a NO_2 background gas at 600 K and subsequently annealed to 900 K thus forming similar SnO_2 crystallites as was observed by STM. A value of 486.0 eV BE was found. In similar studies for Sn-oxide films on Pt(100) generated by oxidation with ozone, 485.5 eV for Pt-O-Sn covalent, and 486.5 eV for tin oxide at 300 K have been reported.[26] Our value is by about 0.3 eV lower then the reported values for bulk SnO_2 surfaces, but 0.4 eV higher than for SnO surfaces. Because the STM data shows directly the formation of SnO_2 crystallites, and such a stoichiometry for the multilayer films comes from UPS and HREELS studies and is discussed below we assign this peak to Sn^{4+}. Spectra for the oxidized alloy surfaces, i.e., monolayer tin-oxide films, could not be fitted satisfactorily by convolution of Sn^0 and Sn^{4+} peaks alone. Therefore, a third peak at an intermediate BE was fitted to the spectra, as was done in previous studies of Sn-oxide/Pt interfaces.[23] Keeping the BE's of the metallic and Sn^{4+} peaks fixed and assuming that all three peaks have the same full width at half maximum (FWHM), gave a best peak position for this intermediate peak at 485.0 eV BE. This peak was assigned previously to an oxidized form of Sn with a BE energy less than SnO and was labeled as ''quasimetallic'' by Rotermund and co-workers.[33]

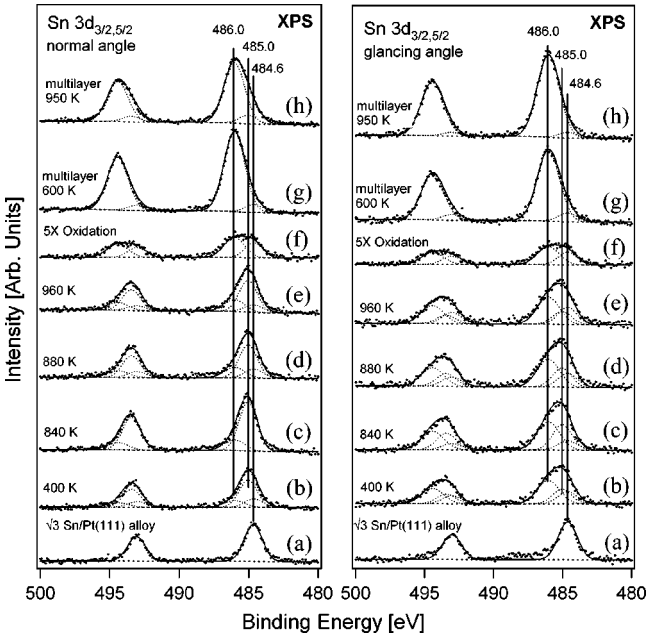

FIG. 6. Sn $3d$ XPS spectra obtained at normal exit angles (left panel) and glancing exit angles (right panel). XPS spectra are shown for (a) $(\sqrt{3}\times\sqrt{3})R30°$ Sn/Pt(111) surface alloy, (b) after a saturation dose of NO_2 on the $(\sqrt{3}\times\sqrt{3})R30°$ Sn/Pt surface alloy at 400 K, and after annealing to (c) 840, (d) 880, and (e) 960 K. (f) Spectra after five oxidation and annealing cycles. (g) Multilayer tin-oxide film prepared at 600 K and (h) after annealing to 950 K. The spectra are decoconvoluted into three peaks at 486.0 eV (Sn^{4+} oxidic state), 485.0 (quasimetallic state), and 484.6 eV BE (metallic state).

Significant differences in relative intensities of the Sn peak components were observed for XPS data collected at the two exit angles. At a glancing angle, the Sn^{4+} component of the peaks for all annealing temperatures is strongly enhanced. The metallic component at a glancing angle also appears to be enhanced a little, but far less so than the oxidic component. These increases are all on the expense of the quasimetallic component that was dominant at normal exit angles. This result may be rationalized if the oxidic Sn component originates from the very surface layer, the quasimetallic Sn from a narrow interface region between the oxide layer and the substrate, and the metallic Sn component from subsurface Sn alloyed with the Pt substrate. In this scenario the quasimetallic component would be attenuated the most at glancing exit angles compared to normal exit angles. Furthermore, if the oxide layer is ''open,'' i.e., holes in the surface layer allows to ''see'' the second layer at normal angles, as for example is suggested in the model in Fig. 5, then some of the quasimetallic Sn may be present at the very surface.

This explains a strong intensity at normal angle for this component, and at the same time the strong attenuation of the photoelectrons at glancing exit angles. The fact that the quasimetallic state is dominant at normal exit angles despite the fact that it may not be in the topmost layer clearly indicates that most of the chemically altered Sn is in a quasimetallic state rather than in a Sn^{4+} state. For the model proposed in Fig. 5 for the ordered (4×4) structure, the Sn atoms that remained alloyed with the Pt substrate have less oxygen bonds than the Sn in the overlayer. This would also indicate that the quasimetallic component in XPS arises from Sn atoms alloyed in the surface layer. The alloyed Sn atoms have effectively a SnO stoichiometry. The fact that Pt atoms surround them may give them an even more metallic character than what would be expected for SnO. The ratios of the deconvoluted peak areas between the quasimetallic and the oxidic tin does not significantly change with increasing annealing temperature between 880 and 950 K and remains around 2.4 to 2.8. According to the model for the (4×4) overlayer structure depicted in Fig. 5, 0.25 ML Sn is present in a (2×2) Sn/Pt alloy as quasimetallic Sn. Thus only $\sim$0.1 ML Sn should be present as Sn^{4+} in the overlayer. This is less than what is indicated in the model in Fig. 5. However, STM images often show areas that have many vacancies in the (4×4) structure, which may account partly for the discrepancy. Also, the reported ratio between Sn^{4+} and quasimetallic tin contains a significant margin of error, because it critically depends on the deconvolution of the XPS spectra that includes some freedom in the selection of the appropriate procedure.

Interestingly, if the same surface is repeatedly oxidized and annealed, then the oxidic component, and to a lesser extent the metallic component, increases. It is known from previous STM studies[3] that such a treatment always just results in a monolayer oxide that uniformly covers the surface. If we repeat the oxidation and annealing cycles five times we reach a surface that does not exhibit any quasimetallic component in its XPS spectrum. Rather, it can be entirely explained by an oxidic and metallic Sn component alone. This is shown in Fig. 6(f). The LEED pattern of this surface showed some similarities to structure II described in Ref. 3. This structure was explained by an incommensurate tin-oxide film that homogeneously covered the surface. The fact that it is an incommensurate film shows some independence between the tin-oxide film and the platinum substrate. It is possible in such a case that all Sn—O bonds are within the film and there are no oxygen bonds to Sn atoms that are still alloyed with the Pt substrate. This interpretation would support our assignment that the quasimetallic Sn component is due to oxygen bonds to Sn atoms that are alloyed within the Pt surface. The metallic Sn component is due to Sn in the Pt substrate that segregates to the surface and forms a Sn/Pt interface alloy between the Pt substrate and the oxide film. Covering the surface with an oxide layer changes the thermodynamics of the system, and driving forces such as minimizing surface energy and strain are altered. Therefore it cannot be assumed *a priori* that Sn still forms an ordered alloy with the same composition and structure at the Pt/Sn-oxide film interface. Since the exchange energies between Sn and Pt are unchanged, it can be assumed that Sn still likes to surround itself with Pt, which may result in an ordered structure at the interface if enough Sn is available.

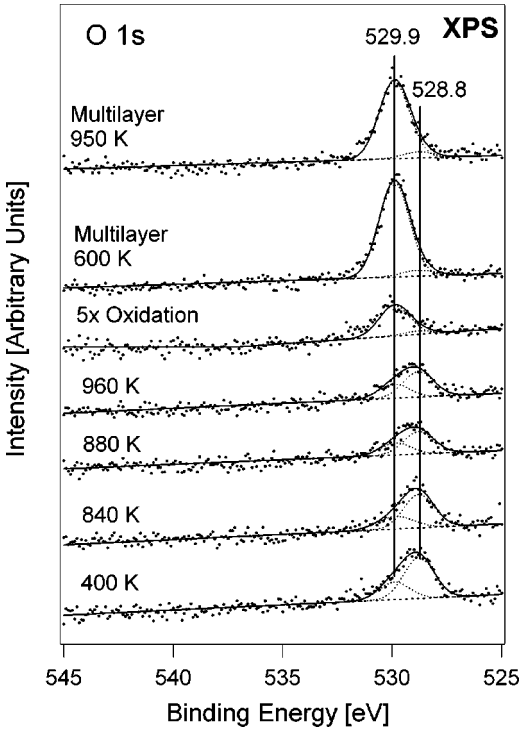

FIG. 7. O 1*s* XPS spectra for an oxidized $(\sqrt{3}\times\sqrt{3})R30°$ Sn/Pt(111) surface alloy after a saturation dose of NO_2 on the alloy at 400 K and annealing of this surface to 840, 880, and 960 K. Spectra after five oxidation and annealing cycles of the monolayer oxide, and for multilayer tin-oxide films prepared at 600 K and annealed to 950 K, are also shown. The O 1*s* peak is decomposed into two components at 529.8 and 528.8 eV BE.

In summary, we conclude that oxidized Sn on top of the substrate give rise to a Sn^{4+} species. The quasimetallic tin component arises from tin remaining alloyed with Pt in the surface layer but also forming bonds to oxygen atoms. The apparently reduced oxidic state of the quasimetallic tin compared to Sn^{2+} is a consequence of its chemical environment. Thus we conclude that quasimetallic Sn is Sn(II) in a Pt environment.

XPS spectra for the O 1*s* peak are shown in Fig. 7. The O 1*s* peaks were decomposed into two components. A Gaussian line shape was fitted to the O 1*s* signal of the multilayer Sn-oxide film and the peak position (529.9 eV) and FWHM (1.4 eV) of this peak was assumed to correspond to one component. These values were subsequently kept constant and used as one component in fitting spectra of the oxidized alloy. Use of a second peak at 528.8 eV BE and 1.4 eV FWHM allowed us to fit all the spectra for the Sn-oxide monolayers.

We assign the highest BE O 1*s* peak to SnO_2 and the lower BE peak to oxygen bound to quasimetallic tin. Repeated oxidation resulted in an increased intensity and, in particular, an increase of the O 1*s* component belonging to SnO_2. For the surface that had been oxidized five times the O 1*s* peak can be fit by only one peak in agreement with the

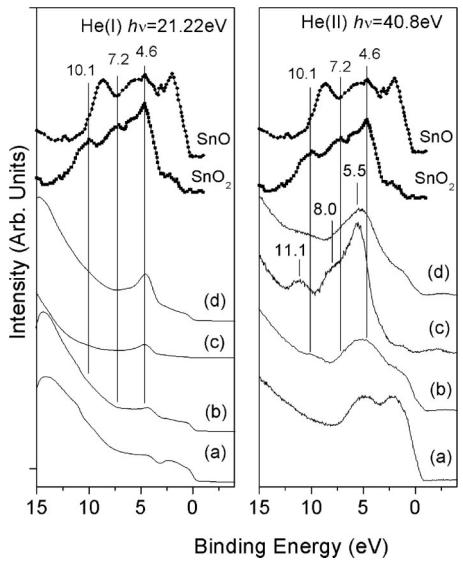

FIG. 8. He I (left panel) and He II (right panel) UPS spectra for (a) $(\sqrt{3}\times\sqrt{3})R30°$ Sn/Pt(111) surface alloy, (b) monolayer tin-oxide film obtained by oxidizing the surface alloy and subsequently annealing to 900 K, (c) multilayer tin-oxide film prepared at 600 K, and (d) after annealing to 950 K. For comparison X-ray induced valence band spectra for SnO and SnO_2 are reproduced from Ref. 26.

XPS data for the Sn-signal that only showed metallic and oxidic tin but no quasimetallic tin.

C. UV Photoelectron spectroscopy (UPS)

The valance band structure of tin-oxide monolayers and multilayers films was measured by UPS. The band gap for SnO is in the range of 2.5–3 eV compared to 3.6 eV for SnO2. Thus valence band spectra of the two materials should clearly discriminate between the two. Analysis of the valence-band structure has been reported to allow discrimination between SnO and SnO_2.[26,27,32] The valence-band spectra of SnO (Refs. 30, 34, 35) and SnO_2 (Refs. 31, 36) show significant differences, with the most notable being a large peak at ~2 (Ref. 26) or ~3 eV (Ref. 35) below the Fermi edge for SnO. The first prominent peak appears at $E_B=5$ eV for SnO_2. It was proposed[26] that the Sn $5s$-derived levels that are part of the conduction band for SnO_2 become part of the valence band for SnO, and these electron states are the origin for the low BE peak of SnO. For SnO_2, the peak at 5 eV is O $2p$ derived. In Fig. 8, we reproduce x-ray induced valence band spectra for SnO and SnO_2.[26] These data were chosen because they directly compare the valence band spectra for SnO and SnO_2. Cox *et al.*[37] reported peaks for the He II UPS spectra for polycrystalline SnO_2 at 4.8, 7.4, and 11.2 eV below the Fermi edge.

The energy distribution curves of photoelectrons excited by He I (21.2 eV) and He II (40.8 eV) photons are shown in Fig. 8. The valence band spectra for the different monolayer film structures do not exhibit any clear differences and are mainly dominated by photoelectrons from the metal. The He II spectra of the multilayer films before annealing resembles the SnO_2 spectra with a low energy peak at 5 eV BE. No peak at 2–3 eV BE was detected, indicating that no SnO is present in the film. The photoelectrons from the metal substrate are effectively attenuated by the multilayer film so that no electrons from the Fermi edge are detected and so before annealing the surface is uniformly covered by a presumably disordered SnO_2 film. After annealing to 950 K, a shoulder at the Fermi edge was observed. The main peak, however, remains at 5 eV. Photoelectrons from the Fermi edge are observed consistent with STM observations that show islanding, i.e., formation of SnO_2 crystallites, and thus areas are exposed that are only covered by a monolayer tin-oxide wetting layer.

The work function ϕ for monolayer and multilayer tin-oxide films was deduced by the onset of electron emission in the He I spectra (not shown). Using this method, we find work function values of $\phi_{Pt(111)}=5.6$ eV for Pt(111), $\phi_{\sqrt{3}alloy}=5.3$ eV for the $(\sqrt{3}\times\sqrt{3})R30°$ Sn/Pt alloy surface, $\phi_{mono}=5.2$ eV for the monolayer tin-oxide films, and $\phi_{multi,600\ K}=5.1$ eV and $\phi_{multi,960\ K}=5.3$ eV for multilayer films before and after annealing to 960 K, respectively. For multilayer SnO_2 films the work function is 0.1 eV lower than for monolayer tin oxide films. The value we derived for SnO_2 films is however higher by 0.6 eV than what was previously reported for $SnO_2(110)$ single crystal surfaces.[37] The increase of the work function after annealing is again attributed to islanding and exposure of monolayer tin oxide wetting layers at the surface.

D. High-resolution electron energy loss spectroscopy (HREELS)

Vibrational spectra using HREELS were taken for oxidized surface alloys and for different surface structures resulting from repeated oxidation and annealing of the surface.[3] In addition, HREELS was performed on multilayer tin-oxide films grown at 600 K and after annealing to 950 K. Surface optical phonons of ionic crystals can be observed by HREELS, and Cox *et al.*[38] reported two single-phonon losses at 339 and 694 cm^{-1} for the $SnO_2(110)$ surface. Studies on polycrystalline SnO_2 also only showed two loss peaks at 290 and 669 cm^{-1}.[37] Using the necessary condition $Re[\varepsilon(\omega)]=-1$ for observing energy loss peaks at an energy of ω, peak positions were predicted at frequencies of 270, 350, 725 cm^{-1} (for $E\perp c$, i.e., the electric vector normal to the [001] c axis of the crystal), and 704 cm^{-1} (for $E\|c$) (Ref. 37) by utilizing a dielectric function that was derived by using a classical oscillator analysis to fit infrared reflectance data from a $SnO_2(110)$ sample.[39] In specular HREELS, energy loss peaks only occur for those modes with a dipole moment normal to the surface and so one expects to observe different loss peaks for different crystal orientations. However, it is worth pointing out that the rutile (011) surface is not normal to the (110) surface. Therefore, there will always be components of the dipole moment that are normal to both surfaces and thus the same phonon modes will be recorded in HREELS. Relative differences in intensity between different modes are however expected. Experiments on $SnO_2(110)$ (Ref. 38) and polycrystalline SnO_2 (Ref. 37) showed that

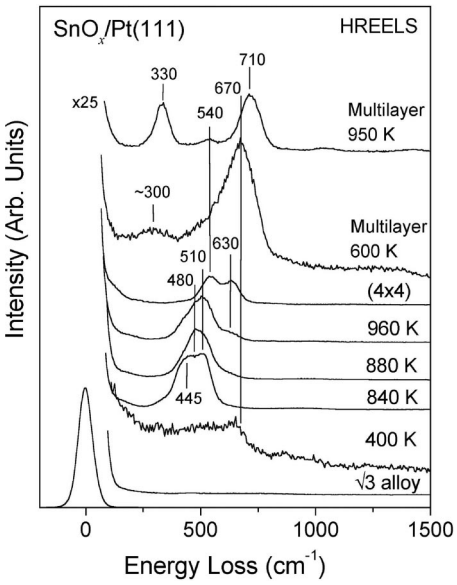

FIG. 9. HREELS spectra for the $(\sqrt{3}\times\sqrt{3})R30°$ Sn/Pt(111) alloy surface after a saturation dose of NO_2 on the alloy at 400 K and after annealing to 840, 880, and 960 K. A spectrum of a surface exhibiting a clear (4×4) LEED pattern after a second oxidation and annealing cycle is shown. Spectra for multilayer oxides as prepared at 600 K and after annealing to 950 K are also displayed.

only two loss peaks are observed experimentally. For the isostructural rutile TiO_2 (110) surface, which has similar phonon modes, three modes were observed.[40]

Figure 9 shows the HREELS spectra for several different surfaces. After oxidizing a Sn/Pt surface alloy at 400 K, a broad shoulder appears in the HREELS spectrum, extending from the elastic peak to about 700 cm^{-1}. Annealing to 840 K, which is known to cause desorption of oxygen and formation of a diffuse LEED pattern, resulted in a broad peak in HREELS, which is a superposition of at least two peaks, with a best fit provided by three peaks at 410, 460, and 520 cm^{-1}. Annealing to 880 K, which resulted in a structure-I LEED pattern (following the nomenclature of Ref. 3), caused a narrowing in the HREELS peak. This is mainly due to a decrease of the 410 cm^{-1} component and increase of the 470 cm^{-1} component of the broad peak observed for lower annealing temperatures. Further annealing to 960 K and formation of a (4×4) structure results in the appearance of a new peak at 630 cm^{-1}. The spectrum characteristic of this structure can be better observed if the sample is reoxidized and annealed. This treatment results in a sharp and clear (4×4) LEED pattern. For this surface only two peaks are observed, one at 540 cm^{-1} and another at 630 cm^{-1}. Thus, the (4×4) structure shows a distinctively different vibrational spectrum from the other monolayer oxide films. This confirms the impression from STM studies that this film compromises a very different atomic arrangement compared to the other oxide monolayers described in Ref. 3. Both previously discussed models for the (4×4) structure, i.e., zero-dimensional Sn—O pseudomolecules and the model proposed above of one-dimensional —Sn—O— chains, potentially have unique vibrational excitations. It is possible that one of the two peaks may not arise from the (4×4) structure. STM measurements show that many disordered regions may be present at the surface even though a clear (4×4) LEED pattern is observed.

Sn-oxide multilayers show a very different vibrational spectrum compared to the monolayer films. Prior to annealing two broad peaks are present at ~300 and 670 cm^{-1} which corresponds to the values reported for polycrystalline SnO_2 samples.[37] The peak at 300 cm^{-1} is, however, very weak. Annealing this film to 950 K forms well defined SnO_2 crystallites with two peaks observed at 330 and 710 cm^{-1}. These loss energies correspond closely to those observed for the SnO_2(110) surface.[38] Weak overtones due to multiple phonon losses are observed at ~1050 and ~1450 cm^{-1}. These overtones are much weaker than those observed on bulk oxide surfaces. This is ascribed to the reduced dimensions of the SnO_2 films. The reason for the shifting of the peaks to higher energies upon annealing is not clear. We speculate that it is a consequence of grain coarsening and the formation of well-ordered crystallites. Nevertheless, the close resemblance of spectra for the multilayer films with the previous reported data for SnO_2 further supports the assignment of rutile SnO_2 to both multilayer films, grown at 600 K and formed after annealing to 900 K, respectively. A weak peak appears at ~520 cm^{-1} after annealing that corresponds to a peak observed for the oxidized alloy surfaces and thus is associated with the wetting layer.

E. Electron energy loss spectroscopy (ELS)

ELS studies were also performed with incident electron energies of $E_p=30$ and 100 eV. Such spectra are displayed in Fig. 10. The monolayer tin-oxide films show only small differences from the clean Sn/Pt alloy surface. Repeated oxidation causes some small changes. Weak, broad peaks at 5.0 and 5.4 eV are marked in Fig. 10. These may correspond to interband transitions or plasmon excitations. For multilayer tin-oxide films, there is an ''onset'' in transition energies at ~3.0 eV for the samples prepared at 600 K and a sharper onset at ~3.8 eV after annealing to 960 K. This onset energy closely coincidences with the band gap for SnO_2 of 3.6 eV.[41–43] Higher loss energies cause electron excitation into the conduction band. The broad onset energy for the preannealed sample indicates a higher defect density. These studies show that the SnO_2 crystallites, even though they are only ~3 monolayers (0.7 nm) thick, posses a well-defined band gap. For the annealed film three additional weak loss peaks can be identified at around 4.8, 6.0, and 8.2 eV. Loss peaks at 6.4 and 8.4 eV were previously reported for SnO_2 and assigned to interband transitions.[6]

IV. SUMMARY

Tin-oxide films grow epitaxially on Pt(111) substrates with a strong structural relationship between the oxide and the metal surface lattice. The strong oxide interaction with the Pt substrate results in a coincidence lattice for the monolayer-thick wetting layer. Thicker oxide films grow as well-defined crystallites if the sample is annealed. This may be described as a Stranski-Krastanov growth mode. The ob-

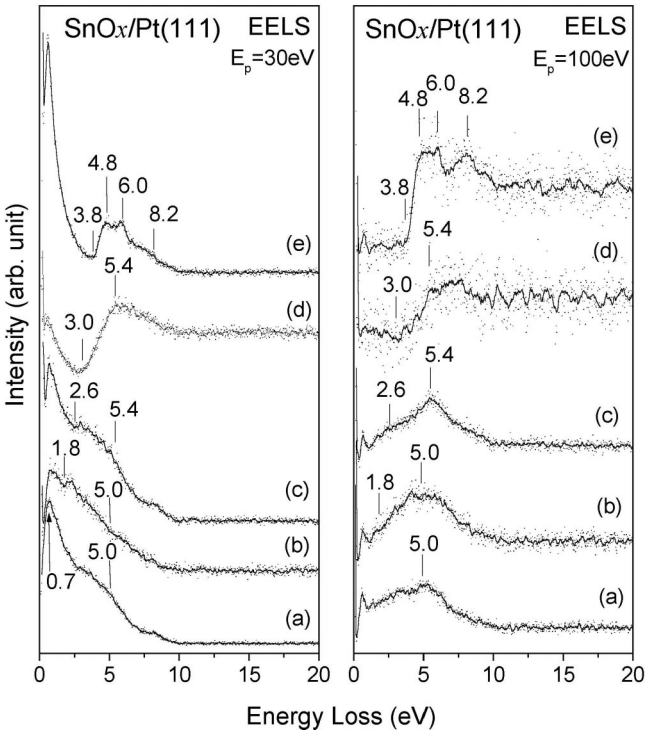

FIG. 10. ELS spectra obtained at incident electron energies of 30 eV (left panel) and 100 eV (right panel) are displayed for (a) the $(\sqrt{3}\times\sqrt{3})R30°$ Sn/Pt(111) surface alloy, (b) monolayer tin-oxide films obtained by a saturation dose of NO_2 at 400 K onto the $(\sqrt{3}\times\sqrt{3})R30°$ Sn/Pt(111) alloy surface and annealing to 900 K, (c) monolayer oxide films obtained by five repetitions of the NO_2 dosing and annealing procedure, (d) multilayer tin-oxide film prepared at 600 K, and (e) after annealing to 950 K.

served (4×4) LEED pattern is entirely due to the wetting layer and not the crystallites. In other reports, such as on the growth of tin-oxide on Au(111),[6] a coincidence LEED pattern for a multilayer oxide film was also reported after annealing. We propose that this is also a result of an ordered wetting layer, rather than a consequence of a uniform oxide film as asserted previously. This proposal, however, needs to be confirmed by appropriate real space data. These data provide additional evidence for the importance of Stranski-Krastanov growth of oxide films on metal substrates. Strong interaction between the metal and the oxide favors such a growth mode.

The preference of the oxide to grow in registry with the metal substrate results in a crystallographic orientation of the crystallites to reduce the misfit between substrate and oxide. For the growth of SnO_2, this results in the formation of a rutile structure oriented with the (011) surface parallel to the Pt(111) substrate. This exposes a higher energy surface of the oxide crystallites. Forming an interface with a small lattice mismatch to the substrate, and thus reducing the strain in the crystallites, presumably compensates for the increased surface energy of the (011) surface compared to, for example, the (110) surface of the SnO_2 crystallites. Thus, oxide surfaces other than those with the lowest free energies can be stabilized in thin oxide films on metal substrates. This conclusion is directly relevant to the chemistry, structure, and properties of oxide surfaces at metal/oxide interfaces relevant to catalysis, sensors, and nanoscale devices.

XPS spectra of monolayer Sn-oxide films were interpreted by considering the structural information from STM data. We concluded that the so-called ''quasimetallic'' state is due to oxidized Sn that stayed alloyed with Pt in an alloy surface. Thus the Pt/tin-oxide interface is complex with no atomically sharp transition. Repeated oxidation and annealing, however, can result in formation of a sharp interface between the Pt metal substrate and a tin-oxide monolayer. In this case, no quasimetallic Sn is detected in XPS and an incommensurate tin-oxide film is observed by STM and LEED.[3] This demonstrates once again that multiple, metastable configurations for monolayer-oxide films on metals can exist.

HREELS spectra also show distinct chemical differences between monolayer and multilayer oxide films. This is a result of the strong interaction of the Pt substrate with the oxide that results in oxide films with different stoichiometry and structure compared to bulk oxide surfaces. The ELS and UPS spectra clearly show features characteristic of rutile SnO_2 crystals. These data strongly support the assignment for the multilayer films and the crystallites observed by STM as rutile SnO_2. These techniques appear to be much better suited to discriminate between different tin-oxygen stoichiometries in the oxide films than XPS. These spectroscopic techniques also indicate that crystallites only 2–3 layers (0.7 nm) thick of tin-oxide grown on Pt are sufficient to regain bulk-oxide-like properties.

ACKNOWLEDGMENT

This work was partially supported by the Analytical and Surface Chemistry Program in the Division of Chemistry, National Science Foundation (NSF).

*Email address: koel@usc.edu

[1] O. Dulub, W. Hebenstreit, and U. Diebold, Phys. Rev. Lett. **84**, 3646 (2000).
[2] D. R. Jennison, O. Dulub, W. Hebenstreit, and U. Diebold, Surf. Sci. Lett. **492**, L677 (2001).
[3] M. Batzill, D. Beck, and B. E. Koel, Phys. Rev. B **64**, 245402 (2001).
[4] W. Weiss and M. Ritter, Phys. Rev. B **59**, 5201 (1999).
[5] W. Ranke, M. Ritter, and W. Weiss, Phys. Rev. B **60**, 1527 (1999).
[6] Y. Zhang and A. J. Slavin, Phys. Rev. B **49**, 2005 (1994).
[7] S. Surnev, L. Vitali, M. G. Ramsey, F. P. Netzer, G. Kresse, and J. Hafner, Phys. Rev. B **61**, 13945 (2000).
[8] S. Surnev, G. Kresse, M. G. Ramsey, and F. P. Netzer, Phys. Rev. Lett. **87**, 086102/1-4 (2001).
[9] S. Shaikhutdinov, M. Ritter, and W. Weiss, Phys. Rev. B **62**, 7535 (2000).
[10] T. Matsumoto, S. Hsieh, M. Batzill, and B. E. Koel (unpublished).
[11] N. Saliba, D. Beck, C. Baur, M. Batzill, S. Hsieh, T. Matsumoto, and B. E. Koel (unpublished).
[12] M. Hoheisel, S. Speller, W. Heiland, A. Atrei, U. Bardi, and G.

Rovida, Phys. Rev. B **66**, 165416 (2002).
[13] A. Atrei, U. Bardi, G. Rovida, M. Torrini, M. Hoheisel, and S. Speller, Surf. Sci. **526**, 193 (2003).
[14] M. T. Paffett and R. G. Windham, Surf. Sci. **208**, 34 (1989).
[15] D. Beck, M. Batzill, C. Baur, and B. E. Koel, Rev. Sci. Instrum. **73**, 1267 (2002).
[16] N. Swami, H. He, and B. E. Koel, Phys. Rev. B **59**, 8283 (1999).
[17] M. Batzill, A. Chaka, and U. Diebold, Europhys. Lett. **65**, 61 (2004).
[18] J. Oviedo and M. J. Gillan, Surf. Sci. **463**, 93 (2000).
[19] F. Jensen, F. Besenbacher, E. Lægsgaard, and I. Stensgaard, Phys. Rev. B **41**, 10233 (1990).
[20] M. Taniguchi, K. Tanaka, T. Hashizume, and T. Sakurai, Surf. Sci. **262**, L123 (1992).
[21] L. Eierdal, F. Besenbacher, E. Lægsgaard, and I. Stensgaard, Ultramicroscopy **42-44**, 505 (1992).
[22] K. Tanaka, Y. Okawa, Y. Matsumoto, and T. Fujita, Surf. Sci. **377-379**, 744 (1997).
[23] D. I. Jerdev and D. E. Koel, Surf. Sci. **492**, 106 (2001).
[24] Y. Li, M. R. Voss, N. Sawami, Y.-L. Tsai, and B. E. Koel, Phys. Rev. B **56**, 15982 (1997).
[25] N. A. Saliba, Y.-L. Tsai, and B. E. Koel, J. Phys. Chem. B **103**, 1532 (1999).
[26] J. M. Themlin, M. Chtaïb, L. Henrard, P. Lambin, J. Darville, and J. M. Gilles, Phys. Rev. B **46**, 2460 (1992).
[27] R. Sanjinés, C. Coluzza, D. Rosenfeld, F. Gozzo, P. Alméras, F. Levy, and G. Margaritondo, J. Appl. Phys. **73**, 3997 (1993).
[28] R. Sanjinés, D. Rosenfeld, F. Gozzo, P. Alméras, L. Pérez, F. Lévy, G. Margaritondo, and W. H. Schreiner, Surf. Interface Anal. **22**, 372 (1994).
[29] D. A. Ashbury and G. B. Hoflund, J. Vac. Sci. Technol. A **5**, 1132 (1987).
[30] V. Jiménez, A. Fernández, J. P. Espinós, and A. R. González-Elipe, Surf. Sci. **350**, 123 (1996).
[31] V. M. Jiménez, J. A. Mejías, J. P. Espinós, and A. R. González-Elipe, Surf. Sci. **366**, 545 (1996).
[32] V. M. Jiménez, J. P. Espinós, and A. R. González-Elipe, Surf. Sci. **366**, 556 (1996).
[33] H. H. Rotermund, V. Penka, L. A. DeLouise, and C. R. Brundle, J. Vac. Sci. Technol. A **5**, 1198 (1987).
[34] V. M. Jiménez, G. Lassaletta, A. Fernández, J. P. Espinós, F. Yubero, A. R. González-Elipe, L. Soriano, J. M. Sanz, and D. A. Papaconstantopoulos, Phys. Rev. B **60**, 11171 (1999).
[35] C. Lau and G. K. Wertheim, J. Vac. Sci. Technol. **15**, 622 (1978).
[36] R. G. Egdell, S. Eriksen, and W. R. Flavell, Solid State Commun. **60**, 835 (1986).
[37] P. A. Cox, R. G. Egdell, C. Harding, W. R. Patterson, and P. J. Tavener, Surf. Sci. **123**, 179 (1982).
[38] P. A. Cox, R. G. Egdell, W. R. Flavell, and R. Helbig, Vacuum **33**, 835 (1983).
[39] R. Summitt, J. Appl. Phys. **39**, 3672 (1968).
[40] M. A. Henderson, Surf. Sci. **355**, 151 (1996).
[41] V. T. Agekyan, Phys. Status Solidi A **43**, 11 (1977).
[42] D. Fröhlich, R. Klenklies, and R. Helbig, Phys. Rev. Lett. **41**, 1750 (1978).
[43] M. Nagasawa and S. Shionoya, J. Phys. Soc. Jpn. **30**, 158 (1971).